On the use of the compression split Hopkinson pressure bar to high strain rate

H. Couque, J. Walker

JOURNAL DE PHYSIQUE IV
Colloque C8, supplément au Journal de Physique III, Volume 4, septembre 1994

On the use of the compression split Hopkinson pressure bar to high strain rate

H. Couque and J.D. Walker

Southwest Research Institute, 6220 Culebra Road, San Antonio, Texas 78228, U.S.A.

Résumé: La réponse en compression d'un cuivre, d'un acier et d'alliages de tungstènes a été obtenue à l'aide de barres d'Hopkinson (split Hopkinson pressure bar) pour des vitesses de déformation variant de 3 x 10^3 à 7 x 10^3 s^{-1}. L'hypothèse de déformation à vitesse constante a été examinée à l'aide de jauges de contrainte placées sur l'échantillon. Au début de la déformation plastique, des vitesses de déformation près de la face avant de l'échantillon supérieures à la vitesse de déformation conventionnelle ont été observées. Cette discontinuité fut confirmée à l'aide de la simulation numérique utilisant un hydrocode d'un essai conduit à 7160 s^{-1}. Les résultats numériques indiquent également une discontinuité de l'état de contrainte impliquant que la réponse du matériau pour des déformations allant jusqu'a 0.1 n'a pas lieu sous un état uniaxial de la contrainte.

Abstract: The compressive response of copper, steel, and tungsten alloys was generated with a split Hopkinson pressure bar technique at strain rates varying from 3 x 10^3 to 7 x 10^3 s^{-1}. Constant strain rate assumptions were examined using specimen surface strain records. During the early stage of the plastic deformation specimen strain rates near the loading interface were found to exceed the conventionally measured strain rate. This discontinuity was confirmed from the simulation of a test conducted at a strain rate of 7160 s^{-1} using a hydrocode. Numerical results also indicate a stress state discontinuity implying that the material response is not a uniaxial state of stress for strain less than 0.1.

1. INTRODUCTION

Technologies for achieving the strain rate regime of 10^3 to 10^4 s^{-1} are of importance to the development of armor/anti-armor, since most of the energy absorbed by the armor, and lost by the penetrator, occurs in this high rate regime. In the case of heavy metal alloy penetrators, knowledge of their ductility, or capacity to sustain large deformation, in this regime is critical. Another application of this regime is that of dynamic fracture, which, for example, is applicable to the assurance of structural integrity in nuclear pressure vessels. In this case, an understanding of the effect of strain rate on the flow stress of the materials in the crack-tip plastic zone is important to the understanding of dynamic fracture processes. The objective of this investigation was to examine the use of the compression split Hopkinson pressure bars (SHPB) [1-3] for testing ductile materials to strain rates exceeding 5 x 10^3 s^{-1}. SHPB compression tests at strain rates from 3 x 10^3 to 7 x 10^3 s^{-1} were conducted with copper, steel, and tungsten alloys specimens of dynamic flow stress varying from 400 to 2500 MPa. Constant strain rate and uniaxial stress state during deformation were examined using specimen surface strain records and from the numerical simulation of a test conducted at a strain rate of 7160 s^{-1} using the HEMP hydrocode [4].

2. EXPERIMENTAL PROCEDURE

High strain rate tests up to a maximum strain rate of about 5.5 x 10^3 s^{-1} were conducted with a conventional SHPB apparatus composed of maraging steel incident and transmitter pressure bars 12.7 mm in diameter. Specimens, 12.7 mm long and 6.3 mm in diameter, were employed. Using this SHPB setup, maximum strain rate tests were conducted by maximizing the particle velocity at the incident bar/specimen loading interface. The maximum particle velocity was obtained for an incident bar stress of 80% of the maraging steel yield stress. To conduct tests at strain rates exceeding 5.5 x 10^3 s^{-1}, without changing the specimen dimensions, a larger incident bar was employed to provide higher particle velocity at the incident bar/specimen loading interface. Using maraging steel incident bars 25.4 mm in diameter (twice the diameter of our conventional SHPB incident bar), the maximum strain rate was increased to 7 x 10^3 s^{-1}. Some specimens were instrumented with two axial strain gages 3.2 mm by 3.2 mm in planar gage size. One strain gage was located 1.5 mm from the incident bar, while a second strain gage was located at the center of the specimen gage section. High strain rate specimens were an annealed OHFC copper, a 4340 steel tempered to 350°C, and three tungsten alloys. The tungsten alloy composition in weight percent and post-processing condition are 90%W-7%Ni-3%Fe as sintered, 91%W-6%Ni-3Co% as sintered, and 91%W-6%Ni-3Co% 25% swaged, and are designated Fe, Co, and swaged Co, respectively.

3. NUMERICAL PROCEDURE

The numerical analysis of the experiment must be done in such a way as to represent the physics that affects the problem. Recent work at SwRI in simulating the conventional SHPB experiment with the HEMP hydrocode has proved successful in reproducing experiments on ceramics [4]. The HEMP hydrocode models elastic and plastic wave propagation in the specimen and bars, and so catches the dynamic nature of the test. Computational analysis gives insight into what the specimen actually undergoes during the experiment.

Transmitting boundaries were implemented in the hydrocode HEMP to shorten the size of the incident and transmitter SHPB bars in the simulations. This option allows the end boundaries of the computational model to absorb incident stress waves (hence, the boundary "transmits" the waves). This was demonstrated by simulating a steel bar 100 mm long and 20 mm in diameter where a pressure loading was applied to one end. Strains were measured at 30 and 70 mm, and output versus time results are given in Figure 1. Results in Figure 1a were obtained with the free-boundary option. The incident compressive-strain pulse passes by the first two gages ($\varepsilon < 0$) and then reflects from the free end of the computational model as a tensile-strain pulse ($\varepsilon > 0$). Figure 1b shows the transmitting boundary option. The compressive-strain pulse passes by the first two gages, but is not reflected, as it has been absorbed by the transmitting boundary. This is the desired behavior.

One experiment was simulated using the numerical grid shown in Figure 2. The grid consists of short incident and transmitter bars, 76.2 mm and 50.8 mm in length, respectively, and the specimen. The zoning for the specimen consisted of 10 zones through the radius and 20 zones in the axial direction. A typical time step was 0.035 µs; the time step was limited by the zone size and sound speed within the specimen.

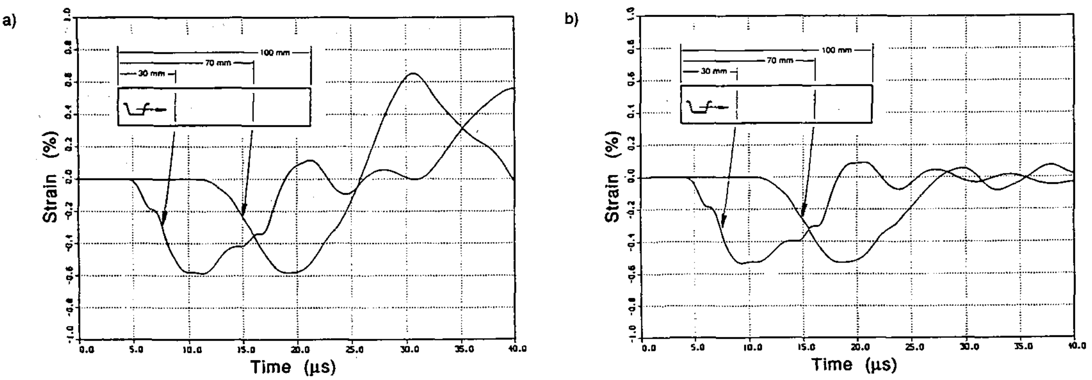

Figure 1. Numerical strain measurements of a pulse travelling in an incident SHPB bar with a) a free boundary, b) a transmitting boundary.

4. EXPERIMENTAL RESULTS

Figure 3 shows typical SHPB stress-strain and strain-rate-strain records of the Fe alloy tested at a strain rate of 5400 s^{-1}. The response up to 0.04 strain occurs under increasing strain rates while the remaining 90% of the specimen deformation occurred at a constant strain rate of 5400 s^{-1}. This constant strain rate is referred as the nominal strain rate of the SHPB.

Figure 4 compares stress-strain responses of the Fe alloy tested with SHPB systems of different incident bar diameters. With both bars transmitting a stress pulse of 80% of the maraging steel yield stress, an increase of the nominal strain rate from 5500 to 7200 s^{-1} was recorded with the increase of the incident bar diameter from 12.7 to 25.4 mm. Using the large incident bar SHPB system, strain rates varying from 6700 to 7200 s^{-1} were reached with the annealed copper, 4340 steel, and Fe alloy; see Table 1.

Table 1. Results of the large incident bar SHPB tests.

Material	Nominal strain rate [s^{-1}]	Flow stress at $\varepsilon = 0.1$ [MPa]
Fe alloy (90%W-7%Ni-3%Fe)	7160	1600
Annealed OHFC copper	6790	400
4340 steel tempered 350°C	6660	1200

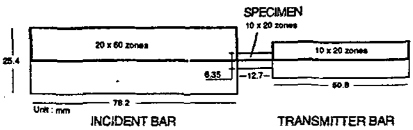

Figure 2. Computer grid for the SHPB model.

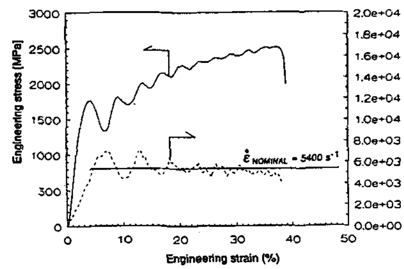

Figure 3. SHPB stress-strain and strain-rate-strain responses in compression of the Fe alloy tested at a nominal strain rate of 5400 s^{-1}.

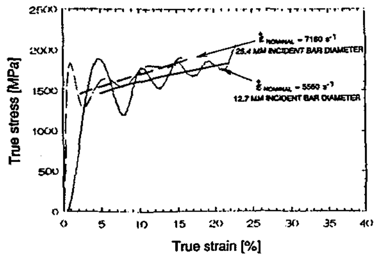

Figure 4. Stress-strain responses in compression of the Fe alloy tested at the maximum loading capacity of the incident maraging bars 12.7 and 25.4 mm in diameter.

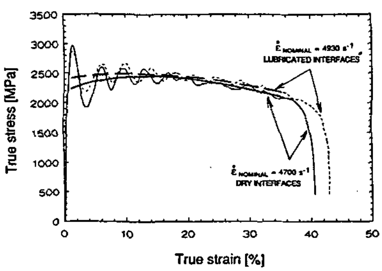

Figure 6. Stress-strain responses in compression of the swaged Co alloy tested with lubricated and dry loading interfaces at nominal strain rate of 4930 and 4700 s^{-1}, respectively.

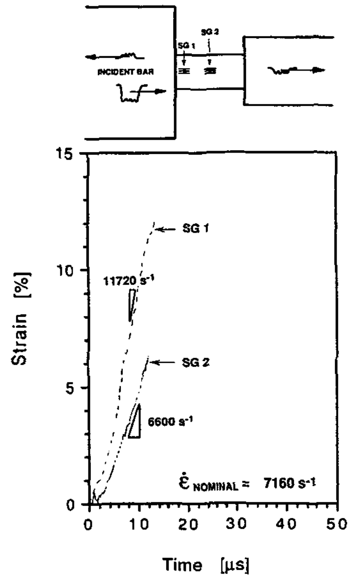

Figure 5. Strain gage records for a Fe specimen tested at a nominal strain rate of 7160 s^{-1}.

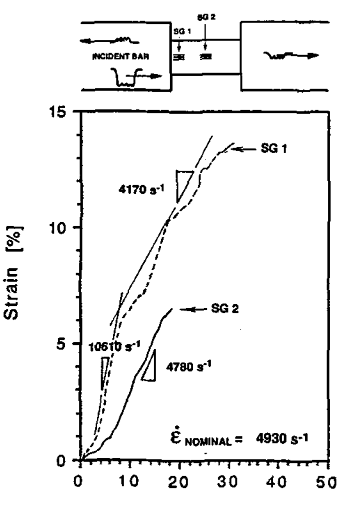

Figure 7. Strain gage records for a swaged Co specimen tested at a nominal strain rate of 4930 s^{-1}.

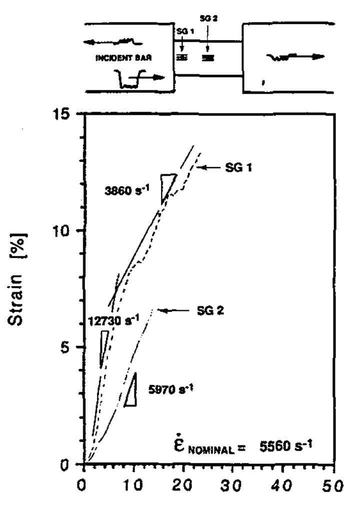

Figure 8. Strain gage records for a Fe specimen tested at a nominal strain rate of 5560 s^{-1}.

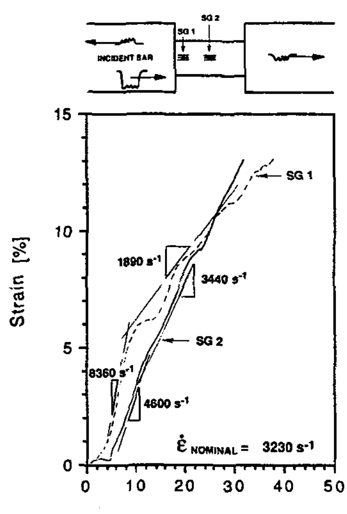

Figure 9. Strain gage records for a Fe specimen tested at a nominal strain rate of 3230 s^{-1}.

To verify that plastic deformation occurred under a constant strain rate, axial strain rate deduced from specimen surface strain records was compared to the nominal strain rate. Figure 5 compares the strain records of the two strain gages for a ductile tungsten alloy tested at a nominal strain rate of 7160 s^{-1}. A strain rate of 11700 s^{-1} was recorded near the specimen interface over a duration of 10 μs, indicating that plastic deformation up to a strain of 0.12 was occurring at twice the nominal strain rate. In contrast, a strain rate on the order of the nominal strain rate was measured at the specimen centerline location.

These results were unexpected and raise questions regarding the use of the SHPB technique to provide plastic response under constant strain rate conditions. In fact, the present view of the mechanics community is that the SHPB non-constant strain rate regime is limited to small strain ($\varepsilon < 0.04$), see Figure 3. This non-constant strain rate deformation of the specimen is assumed to not affect the overall plastic material response. Thus, constitutive models developed with SHPB data assume constant strain rate and uniaxial stress state conditions. With the knowledge that the specimen can locally deform plastically at strain rates twice the nominal strain rate, it is necessary to reconsider the accuracy of the compression SHPB technology as a tool for providing high strain-rate stress-strain response of ductile materials.

To examine whether or not these strain rate discontinuities are related to the lubrication conditions at the specimen/bar interfaces, two tests were conducted with the swaged Co alloy at a strain rate of about 5 x 10^3 s^{-1}. These tests were performed with incident bars 12.7 mm in diameter. In the first experiment, the specimen loading interfaces were unlubricated, while in the second experiment a molybdenum disulfide lubricant was applied to the specimen interfaces. Figure 6 shows the stress-strain responses of the unlubricated and lubricated specimens tested at strain rates of 4700 and 4925 s^{-1}, respectively. Higher yield and flow stresses can be observed, along with an increase of the specimen deformation with the lubricated specimen, and are attributed to the difference in strain rates. Tungsten alloys in the as sintered and swaged conditions display a high strain rate sensitivity when tested in the 10^3 s^{-1} strain rate regime [5], explaining the large increase of the yield stress of 150 MPa with the relatively small strain rate increase of 230 s^{-1}. Since the same striker was used in the two experiments, the loading duration was identical, implying an increase of the deformation proportional to the increase of strain rate. Precisely, the strain rates and final deformations differ by 8%. These results indicate that the same stress-strain response over a strain range exceeding 0.35 will be obtained for unlubricated and lubricated specimens when tested at the same strain rate. It is important to note that these results for moderate strength metals exhibiting low hardening behavior do not transfer to low strength materials exhibiting high hardening characteristics [6]. To examine if strain rate discontinuities prevail along the gage length of the lubricated specimen, local strain measurements were recorded; see Figure 7. Again a high strain rate regime, twice the nominal strain rate, was observed with the strain gage located near the incident bar interface. Consequently, the high strain rate deformation observed near the incident bar interface is inherent to the SHPB loading system.

To investigate if these strain rate discontinuities prevail over the entire 10^3 s^{-1} strain rate regime, two tests at a strain rate of 3230 and 5560 s^{-1} were conducted with the Fe alloy previously tested at 7160 s^{-1}. These tests were performed with the conventional SHPB apparatus. Results are given in Figure 8 and 9. Again a high strain rate, about twice the nominal strain rate, prevails near the front specimen interface (strain gage SG1) at both rates. Strain rates measured with the centered gage SG2 are of the order of the nominal strain rate.

The strain range over which the high strain rate regime prevails increases with the increase of the nominal strain rate. However, a second regime of lower strain rate of the order of the nominal strain rate can be observed. This lower strain rate regime begins where the high rate regime ends. Use of these data require numerical modeling of the experiment. To provide such experimental/analytical technology, the test conducted at a strain rate of 7160 s^{-1} was simulated with the HEMP hydrocode. Details of this investigation are given in the next section.

5. NUMERICAL RESULTS

The experiment conducted with the ductile tungsten alloy at a strain of 7160 s^{-1} was simulated assuming a rate-independent elastic perfectly plastic tungsten alloy with a constant flow stress of 1400 MPa corresponding to the dynamic yield stress at a strain rate of about 7 x 10^3 s^{-1}, a bulk modulus of 278 GPa, and a Poisson's ratio of 0.284. The specimen/bar interfaces were assumed to be perfectly bonded. Figure 10 compares the input incident and output transmitted stress pulses to the experimental data. Excellent agreement is reached for the transmitted stress pulse. This good agreement is further confirmed with calculated specimen strain. Figure 11 shows calculated surface strains averaged over an area 0.64 mm by 0.32 mm at locations representative of the front, center, and back of the specimen. From these records, strain rates were deduced and, along with the experimental data generated with the 3.2 mm by 3.2 mm strain gages, are summarized in Table 2. When compared to the experimental data, Figure 5 and Table 2, strain rates at the center of the specimen gage section are in excellent agreement and differ by only 2 percent. High strain rates are also observed at the incident bar/specimen interface, but underestimate the experimental data by 22 percent. This underestimation is ever greater since the experimental data is an averaged strain rate over a larger area than the numerical data. The computations confirmed the discontinuity in strain rates observed experimentally. In addition, the numerical results indicate that a lower strain rate than the nominal strain rate prevails at the transmitted bar interface for a duration of 20 μs. After 20 μs, or about four round trips of the loading wave, strain rates of the order of the nominal strain rate are observed along the entire gage length. These numerical results are in agreement with the work of Lichtenberger et al. [7] in which a SHPB test conducted at a strain rate of 1.2 x 10^3 s^{-1} was simulated with the HEMP hydrocode. Similar strain rate discontinuities at the specimen interfaces were observed over a deformation of 0.04.

To establish whether the stress-strain response was generated under a uniaxial state of stress, the state of stress from the computations along the specimen gage length at three different radial locations was examined. The state of stress was identified using two stress ratios, the axial-to-yield stress ratio σ_x/σ_o and the radial-to-yield stress ratio σ_r/σ_o. Figures 12a, 13a, and 14a are plots of these stress ratios at times 5, 15, and 25 μs, respectively, in Eulerian coordinates A

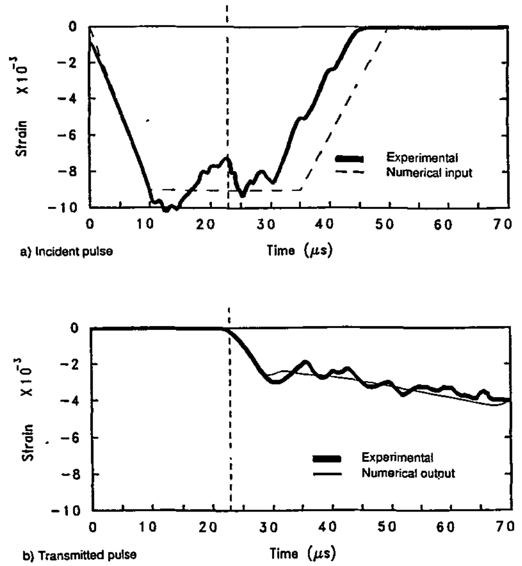

Figure 10. Comparison of experimental and numerical results for the Fe specimen tested at a 7160 s^{-1}: a) incident pulse, b) transmitted pulse.

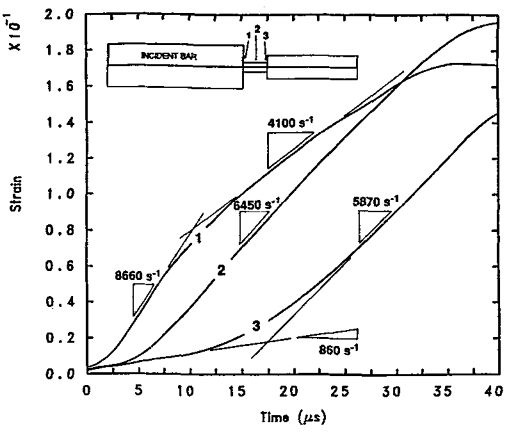

Figure 11. Computed strain-time profile at three locations along the gage length for the Fe specimen tested at a 7160 s^{-1}.

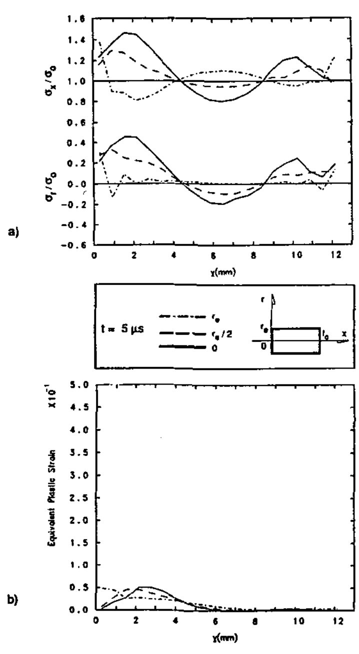

Figure 12. Stress and strain data at 5 μs along the gage length and at three radial locations of the Fe specimen tested at 7160 s^{-1}: a) axial (σ_x) and radial (σ_r) yield stress ratio and b) equivalent plastic strain.

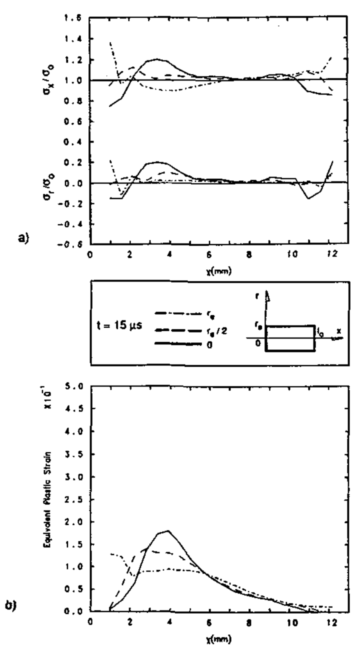

Figure 13. Stress and strain data at 15 μs along the gage length and at three radial locations of the Fe specimen tested at 7160 s^{-1}: a) axial (σ_x) and radial (σ_r) yield stress ratio and b) equivalent plastic strain.

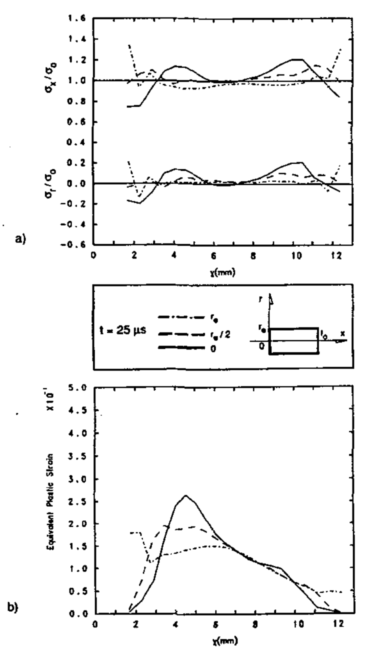

Figure 14. Stress and strain data at 25 μs along the gage length and at three radial locations of the Fe specimen tested at 7160 s^{-1}: a) axial (σ_x) and radial (σ_r) yield stress ratio and b) equivalent plastic strain.

uniaxial state of stress exists when $\sigma_x/\sigma_o = 1$ and $\sigma_r/\sigma_o = 0$. A uniaxial state of strain exists when the ratio (σ_x/σ_r) is equal to about $\upsilon/(1-\upsilon) = 0.4$. Along with these stress ratios, the specimen plastic deformation is indicated in terms of the equivalent plastic strain, see Figures 12b-14b. At 5 µs, a stress state between uniaxial strain and uniaxial stress prevails near the loading interfaces. At 15 µs and 25 µs, when local strain rates scaled with the nominal strain rate (recall Figure 11), a uniaxial state of stress is obtained. A similar evolution of the stress state is observed near the transmitter bar interface. However, for the centered gage section, from 5 µs on the deformation is under a uniaxial state of stress.

Table 2. Calculated and experimental local strain rates for the Fe specimen tested at a nominal strain rate of 7160 s^{-1}.

Location	Time range [µs]	Surface strain rate [s^{-1}]		Exp.-Num. / Exp. [%]
		Experimental	Numerical	
Front	5-10	11720	8660	26
	10-35	-	4100	-
Center	5-10	6600	6450	2.3
	10-35	-	6450	-
Rear	5-12.5	-	860	-
	12.5-25	-	860-5870	-
	25-35	-	5870	

6. DISCUSSION AND SUMMARY

The influence of strain rate and stress state discontinuities on the stress and strain histories deduced from the transmitter and incident bar strain traces [2], respectively, can be assessed as follows. During the first 10 µs, the stress history is read by the specimen/transmitter bar interface and consequently corresponds to the tungsten alloy elastically loaded at a strain rate 9x lower than the nominal strain rate. On the other hand, the strain rate and strain histories, which are read by the specimen/incident bar interface, correspond to the tungsten alloy deforming at twice the nominal strain rate. Consequently, a stress-strain response under a uniaxial state of stress and at a constant strain rate is only reached after 10 µs, at a strain of about 0.07.

These findings indicate that the SHPB technique remains a powerful tool to generate dynamic properties over the 10^3-10^4 s^{-1} strain rate regime since the majority of the plastic deformation is generated under a uniaxial stress state and at a constant strain rate. However, it is important to keep in mind that the stress state and strain discontinuities observed near the front loading interface imply erroneous strain readings. The early strain reading corresponds to the elastic-plastic deformation under a state of uniaxial strain of a shorter specimen of length equal to about 4 mm, see Figure 12a. This shorter specimen, when compared to the tested specimen, amplifies strain readings. In another hand, a state of uniaxial strain will result for a given loading in less axial straining when compared to a state of uniaxial stress. For the test conducted at a nominal strain rate of 7160 s^{-1}, the strain error at 10 µs was estimated to be of the order of -0.02 by considering a specimen of length 4 mm deformed under a uniaxial strain state.

To improve the accuracy of SHPB data generated in the 5 x 10^3 - 10^4 s^{-1} strain rate regime, numerical investigations are needed to simulate more precisely the rate of deformation near the incident/specimen interface and to establish the error on the strain origin of the stress-strain curve. Such investigations will require the use of a material model accounting for strain hardening and an estimate of the strengthening occurring with the evolution of the stress state from uniaxial stress to uniaxial strain in the 10^3-10^4 s^{-1} strain rate regime. Such investigation will also provide insights of compression failure processes such as shear banding.

7. ACKNOWLEDGMENTS

The authors express their thanks to Mr. Arthur Nicholls for his technical support. This investigation was carried out under an SwRI Internal Research Program.

8. REFERENCES

[1] Kolsky, H., *Proc. Phys. Soc.*, B62, (1949) pp. 676-700.
[2] Lindholm, U. S., *J. Mech. Phys. Solids*, Vol. 12, (1964) pp. 317-335.
[3] Frantz C. E., Follansbee P. S. and Wright W.T., High Energy Rate Fabrication (Berman I. and J. W. Editors, 1984) pp. 229-236.
[4] Anderson, C. E., O'Donoghue, P. E., Lankford, J., and Walker, J. D., *Inter. J. Fract.*, Vol 55, (1992) pp. 193-208.
[5] Couque H., Lankford J., and Bose A., *J. Phys.III France 2* (1992) pp. 2225-2238.
[6] Bertholf L. D. and Karnes C. H., *J. Mech. Phys.Solids*, Vol. 23, (1975) pp. 1-19.
[7] Lichtenberger A., Gazeaud G. and Lach E., DYMAT 88 Conference, *J. Phys.*, T.49, Colloque C3, Supplément au n°9, (1988) pp. 589-594.